

On the solidification dynamic of an impacted drop

V. Thiévenaz¹, T. Séon^{1†} and C. Josserand²

¹Institut ∂' Alembert, UMR 7190, CNRS & Sorbonne Universités, Paris, France

²Laboratoire d'Hydrodynamique (LadHyX), UMR7646 CNRS-Ecole Polytechnique, 91128 Palaiseau CEDEX, France

(Received xx; revised xx; accepted xx)

We investigate experimentally the solidification of a water drop during its impact on a sub-zero cooled metallic plate. As the drop impacts the substrate, a first thin layer of ice builds-up and pins the water/ice contact line. This ice layer grows as long as the contact line stays stationary. During this particular time τ_{SCL} the contact angle relaxes to reach a typical de-pinning angle and the solidification front propagates vertically in the spread drop. Experimental measurements of the frozen drop profile and a 1D solidification model allow us to characterize the frozen disc thickness as a function of the control parameters.

Key words:

1. Introduction

When a liquid drop is put in contact of a very cold substrate, either by impact or deposition, the freezing of the liquid can lead to surprising final shapes. It varies from a pointy drop shape when the drop is simply deposited on the substrate (Snoeijer & Brunet 2012) to irregular pancakes when the drop impacts on the substrate (Ghabache *et al.* 2016). Further, because of thermal expansion during the solidification (Wildeman *et al.* 2017) or thermal contraction when the ice becomes cooler (Ghabache *et al.* 2016), the frozen structure can fragment into a myriad of small pieces. In general, these final shapes are the result of the coupling between processes of very different time scales. Indeed, at the short times, we observe a fast free surface deformation of the liquid and its almost immediate adhesion through the formation of a thin layer of ice at the contact of the substrate (Schiaffino & Sonin 1997; de Ruiter *et al.* 2018). On the other hand, the slower dynamics corresponds to the freezing of the bulk liquid, which eventually is accompanied by the retraction of the remaining liquid on the growing ice layer (Gao & Sonin 1994; Marin *et al.* 2014).

Understanding the shape of the frozen structure is in fact crucial in many different contexts, from airplane icing (Baumert *et al.* 2018) to 3D printing (Derby 2010). Although most of the airplane icing configurations concern impact of ice crystal impacts (Vidaurre & Hallett 2009; Hauk *et al.* 2015), the impact of liquid droplets on subfreezing substrates can be of great interest in the dynamics of icing formation (Schremb *et al.* 2018). For instance, it is important to characterize the thickness of the residual ice layer to understand the stability of the frozen structure (Schremb *et al.* 2018). In particular, depending on this thickness and the substrate temperature, the frozen structure can

† Email address for correspondence: thomas.seon@gmail.com

remain stick on the substrate or detach through a self-peeling process (Ghabache *et al.* 2016; de Ruiter *et al.* 2018).

In this paper, we investigate experimentally the freezing of a water film formed by the impact of a water drop on cold substrates. We study the growth of the ice from the substrate in order to characterize the thickness properties of the residual ice layer. The paper is organized as follows: Section 2 is a rapid description of the experimental setup and the measurement techniques involved. Section 3 describes the residence regime, which is the moment when the liquid is out of its wetting equilibrium but remains still and keeps freezing. In Sec. 4 we develop a model of unidimensional solidification of a liquid on a substrate. Finally, Section 5 presents our experimental results relating to the formation of the ice plate that is formed through the residence regime.

2. Experimental setup and qualitative description

The classical drop impact setup consists of a syringe pump pushing liquid through a capillary tube from which the drop falls. As the pumping is slow enough, the size of the drop is entirely controlled by the size of the capillary tube. We used two different tubes of inner diameter 1600 μm and 250 μm leading to drop radii $R=1.9$ mm and 1.2 mm or volumes 30 μL and 7 μL respectively. The impact velocity U_0 is controlled by the height of fall. In our case the height of fall H ranges from 15 cm to 45 cm, so that the impact velocity U_0 ranges from 1.7 m.s^{-1} to 3 m.s^{-1} (following roughly $U_0 = \sqrt{2gH}$). Our substrates are made of blocks ($100 \times 100 \times 30$ mm) of different materials : steel, copper and marble. Each material having their own thermal parameters : λ the thermal conductivity, C_p the heat capacity and $D = \lambda/\rho C_p$ the heat diffusion coefficient, with ρ the density.

The substrate is placed into a bowl and cooled down by pouring a certain amount liquid nitrogen. The minimal temperature reached in this work is around -70°C . Due to the substrate heat capacity and to the bowl thermal isolation, it takes several hours for the system to warm up to room temperature. The change in the substrate temperature is thus much less than 1°C during the time of an experiment which is roughly 1 second. In order to minimize frost formation, the whole system is set inside a regulated atmosphere chamber which allows us to drastically reduce the humidity. The substrate temperature T_s is measured before each experiment using a surface thermometer. The dynamic of the impact is studied using a high-speed camera, and the height profil of the frozen drop is extracted with a polychromatic confocal sensor moving along a translation platform.

At room temperature, as a water drop impacts a solid substrate, it spreads, reaches a maximal radius (Laan *et al.* 2014) and immediately starts to retract back to an equilibrium radius (Bartolo *et al.* 2005; Josserand & Thoroddsen 2016). Figure 1 (a)-(h) shows a sequence of snapshots of a water drop impacting a sub-zero substrate. Here again, the drop spreads rapidly and reaches a maximal spreading diameter (a)-(b). But then the drop does not retract, it is stuck at its maximal diameter (c). This pinning is due to the formation of a thin layer of ice at the substrate/liquid interface during the spreading. On images (c)-(e) the drop is made of a thin layer of ice, attached to the substrate and growing vertically, beneath a thicker layer of water where capillary waves are damping. This remaining water layer is not stable due to its high aspect ratio, so that it still needs to retract in order to reach its , and we observe on (e) that the liquid layer actually started to depin from the edge. Then, the liquid retracts on the ice layer (f), until it reaches its typical equilibrium angle on ice and forms a spherical-cap-shaped drop (g). Eventually, it completely freezes, yielding a pointy ice drop (Marin *et al.* 2014), on top of an ice pancake (h).

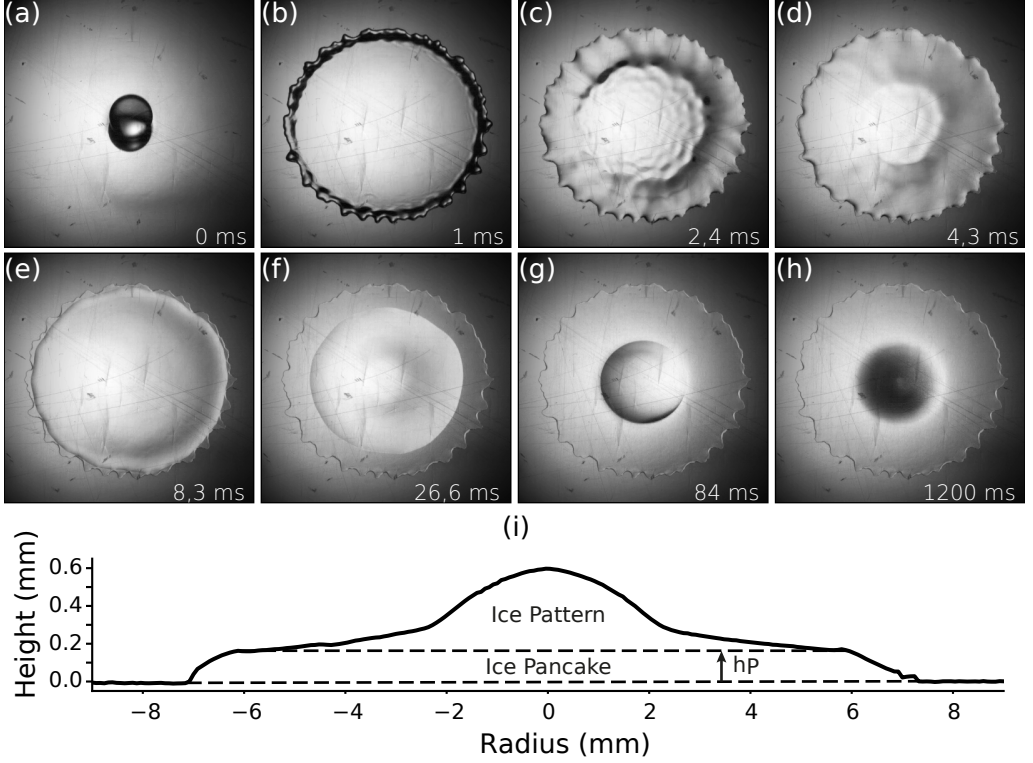


FIGURE 1. Snapshots (a)-(h) show a sequence at different, times indicated on the image, of a drop of water of radius 1.9 mm impacting at velocity 2.6m.s^{-1} on an aluminium substrate at temperature -9°C . (i) is a height profile of the final frozen pattern, measured using the optical profilometry. The aspect ratio is 20, so the real pattern is much flatter.

Figure 1 (i) shows the height profile of the frozen drop (h) obtained by scanning the drop diameter using the optical profilometer. This profile shows clearly two different parts: a quasi-cylindrical plate (the so-called ice pancake), whose thickness is denominated as h_p , on top of which we find an ice pattern, consequence of the water retraction.

This structure with an ice pancake in contact with the impacted solid is found anytime a drop impacts a sub-zero cold surface. On the other hand, the ice pattern that is eventually formed above this ice pancake can exhibit different shapes that will be the subject of future works. The ice pancake is in fact crucial in all relevant applications, in particular for the stability of the frozen drop. Indeed, as the temperature of the ice varies, thermal expansion/contraction generates elastic stress that can lead to the delamination of the pancake (de Ruiter *et al.* 2018) or the formation of cracks (Ghabache *et al.* 2016), both being controlled by the thickness h_p . The aim of the present paper is thus dedicated to the quantification of this thickness h_p .

3. The stationary contact line regime

A crucial difference with the drop impact at non-freezing temperatures is the existence of a regime in which the contact line seems steady, before a dewetting transition and the retraction of the water film on the ice layer (Fig. 1 (b-e)). It is tempting thus to associate the thickness of the ice pancake h_p with the ice layer that would grow by thermal conduction during this steady time. Consequently, in order to validate this theory, we

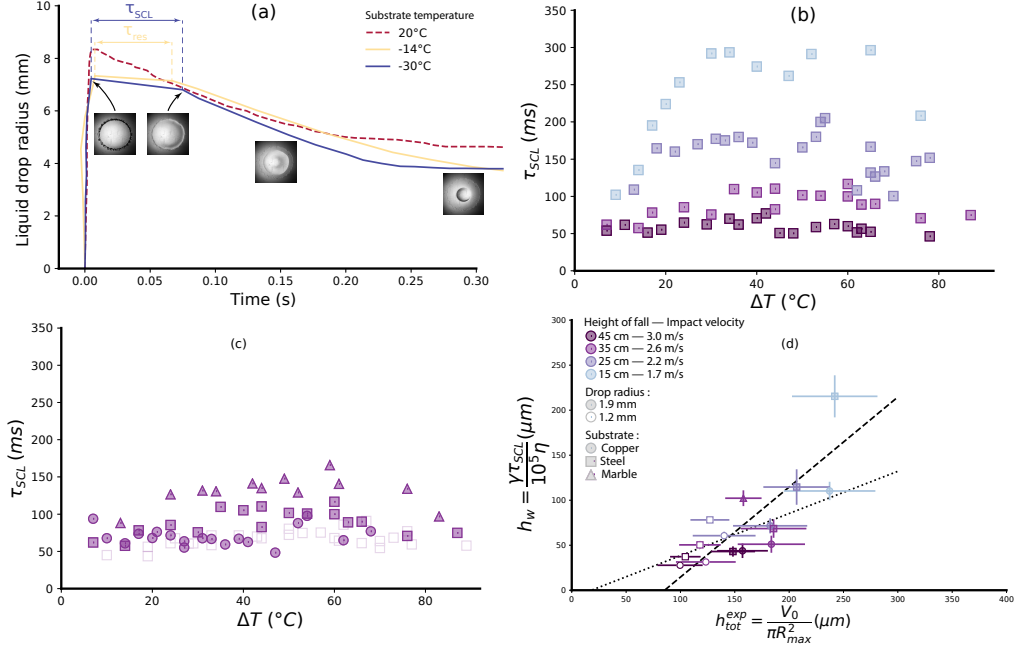


FIGURE 2. (a) The dynamic of spreading and retraction of the drop. The radius of the liquid film is plotted as function of time. The drop spreads in a few milliseconds. Retraction begins immediately at room temperature (red dashed line), and after a time τ_{SCL} below $0^\circ C$. Inset pictures show the aspect of the film on the different stages. On all graphs, impact velocities are represented by colors (light blue for the slowest to dark purple for the fastest), substrate by symbols (circles for copper, squares for steel and triangles for marble) and drop radii by the filling (full symbols for $R = 1.9mm$, empty symbols for $R = 1.2mm$). (b) τ_{SCL} as a function of the temperature ΔT for different impact velocities. The drop radius is $1.9mm$ and the substrate is steel. (c) τ_{SCL} as a function of the temperature ΔT for different substrates. The impact velocity is $2.6m/s$ and the drop radius is $1.9mm$ (full symbols). Results for a drop of $R = 1.2mm$ impacting on steel at the same velocity are shown with empty squares. (d) Theoretical prediction for the water film thickness h_w as a function of its experimental estimation h_{tot}^{exp} . Each point represents a series experiments with given impact velocity, substrate and drop radius. The error bars contain the variations within each series. The dashed line is a linear fit with the slope set to one.

need first to characterize the duration of this regime, that we call stationary contact line (SCL) regime (Rivetti *et al.* 2015). Figure 2 (a) presents the variation of the liquid film radius during an impact, plotted as a function of time, for three different substrate temperatures. The dotted line shows the evolution at room temperature and the two continuous lines at freezing temperature : -14 and $-30^\circ C$. Without freezing (dotted line) the drop spreads rapidly, reaches its maximal diameter and almost instantaneously retracts. The behavior is different when the drop freezes, after having rapidly reached its maximal diameter (illustrated on the curve with the inserts), the stationary contact line regime is observed : the liquid remains attached to the ice layer close to its maximum radius. There the liquid radius varies slightly with time during approximately $6 - 7$ ms before the retraction of the liquid film starts (see insert at the end of the regime). This time between the spreading and the retraction regimes defines the SCL time : τ_{SCL} , as shown on the curves. It appears clearly that the time τ_{SCL} is always much higher than the spreading time (that scales typically as $R/U_0 \sim 1ms$) so that we will neglect the influence of the

spreading dynamics in our theory for the growth of the ice pancake. Finally, we note that the two resident times, for the two different temperatures, seem to be quite close.

Figure 2(b) shows the dependence of τ_{SCL} with the temperature, for different heights of fall and same drop size and substrate material. Instead of substrate temperature T_s , we use $\Delta T = T_m - T_s$, where T_m is the freezing temperature of the liquid (here for water $T_m = 0^\circ \text{C}$ so that $\Delta T = -T_s$ with the Celsius scale), which is *a priori* the relevant temperature here. The first clear observation is that τ_{SCL} reaches a plateau : the resident time is independent of ΔT . The second obvious observation is that the value of this plateau strongly depends on the drop impact velocity and thus on the initial spreading of the liquid film : the larger the maximal diameter at impact, the faster the liquid layer dewets the ice pancake and retracts. These two results suggest therefore that τ_{SCL} might be independent of the heat transfert and due to the proper liquid dynamics.

Figure 2(c) presents the variation of τ_{SCL} with ΔT for three different substrates : marble, steel, copper, and two different drop radii on steel substrat (full and empty squares). In each case, the plateau regime is quickly reached confirming this independence of SCL time with ΔT . As expected, the drop size, as the drop impact velocity, seems to play a role in the selection of the plateau value of τ_{SCL} . What is more surprising here is the variation of the plateau value with the substrate material : τ_{SCL} decreases as the substrate thermal conductivity increases. This appears as a contradiction with the previous result that τ_{SCL} does not depend on the substrat temperature and, thus, seems to be independent of the thermic parameters!

To explain the existence of this delay τ_{SCL} , between spreading and retraction when water freezes we will use the previous work of Rivetti *et al.* (Rivetti *et al.* 2015) on the relaxation of a contact line pinned at the edge of a polymer film. Similarly, we assume here that, in the SCL regime, the time τ_{SCL} is due to the relaxation dynamics of the contact angle θ formed by the liquid film on top the growing ice pancake and pinned at its edge. The initial angle is given by the spreading dynamics (influenced by the drop impact velocity, the substrate wetting angle, and the drop size), and eventually, the receding motion of the line starts when the angle reaches a critical value enabling the depinning of the contact line. In the experiment of Rivetti *et al.*, this angle surprisingly appears to be independent of the liquid parameter and film thickness and is $\theta^* = 4.5^\circ \pm 0.5^\circ$. Moreover, because the liquid film is very thin, its dynamics can be taken in the lubrication regime so that the contact line relaxation follows a self-similar evolution leading to a relaxation time $t_w \propto (h_0 \eta) / \gamma$ with the proportional coefficient function of θ^* (and being about 10^5 in their experiments) Rivetti *et al.* (2015). Finally, as soon as the contact line retracts, they showed that θ increases to a receding contact angle which stays roughly constant during dewetting. In order to show that the same dynamics is at play in our experiments, we compare on figure 2(d) the thickness h_w of the liquid film that would correspond to the relaxation time τ_{SCL} following this self-similar dynamcs (*i.e.* $h_w = \gamma \tau_{\text{SCL}} / (10^5 \eta)$) with the thickness of the water film $h_{\text{tot}}^{\text{exp}}$ formed at the end of the spreading, neglecting ice formation ($h_{\text{tot}}^{\text{exp}} = V_{\text{tot}} / \pi R_{\text{max}}^2$). Remarkably, the experimental data gather along a line of slope 1 suggesting that this relaxation scenario of the the contact line is correct. Moreover, we have used for comparaisn the same value of θ^* than for the polymer films (leading to the 10^5 prefactor for h_w while there is no reason that this value is pertinent for water films. In fact, when trying to fit the best linear fit for the data of figure 2(d), we found an angle slightly different but with no significant improvement eventually compared with the θ^* , so that we have kept this value for the sake of simplicity.

***** This also shed light on a possible universal dewetting angle, that are not far from those observed on by of Rivetti *et al.*. As $h_{\text{tot}}^{\text{exp}}$ is the total height, it is the sum of the ice pancake height and the water film, the intersection of the

dotted line and the x-axis give an estimation of the ice pancake thickness. Finally, as the experiments with different substrat are also on this curve, it confirms our assumption that the dependance of τ_{SCL} with the substrat due to hydrodynamic effects more than thermic effects.

4. Unidimensional solidification model

Since the ice pancake is building during the SCL regime, its thickness results from the product of the building time τ_{SCL} and the building dynamics. In this section we introduce a simplified model that will characterize the main properties of the solidification dynamics involved here. When the liquid enters in contact with the cold substrate, a layer of ice starts almost immediately to grow because of the heat transfer between the liquid and the substrate. The subsequent configuration is thus : a solid substrate in contact with an ice layer growing in water (see schematic of Fig.3 (a)). This dynamic of solidification is reminiscent of the so-called Stefan problem, widely explored as the generic problem of a discontinuous flux at a moving interface (Stefan 1891; Gupta 2003). The Stefan problem however usually concerns only the dynamics of the front separating the two phases (in general liquid and solid) of the same material, with different thermal properties. It assumes semi-infinite phases, which is not coherent with the case of a drop impacting a cold substrate since the ice layer is rather thin. When a solid body is added, the problem becomes more complex. For instance, considering the temperature of the solid to be constant and thus acting only as a fixed temperature boundary condition, leads already to a transcendental equation for the solidification front dynamics (Worster 2000). But, the solid temperature is not constant, because of the heat flux, and thermal properties of the material have to be considered (de Ruiter *et al.* 2018).

Therefore, we will consider here a model coupling three different domains, the substrate, the growing ice layer and the liquid layer *as seen on figure 3 (a)*. The choice of a one-dimensional model is supported by the strong aspect ratio of the drop which resembles a pancake much more than a drop (see Fig.1). In addition, we will assume that the liquid is at the melting temperature T_m . This approximation can be justified both by, again, the small thickness of the liquid pancake and, by the low energy needed to cool the water down to the melting temperature ($C_{pl}(T_d - T_m) \sim 4000 \times 20 \sim 8 \cdot 10^4$ J·kg⁻¹, where C_{pl} is the heat capacity of water and T_d the initial temperature of the drop), compared the latent heat for solidification ($L \sim 3 \cdot 10^5$ J·kg⁻¹). We end up with the heat equations for the temperature field $T(z, t)$ in the substrate (for $z \leq 0$) and in the ice layer (defined by $0 \leq z \leq h(t)$, where $h(t)$ is the height of the ice layer) and a constant temperature in the liquid ($z > h(t)$):

$$\frac{\partial T}{\partial t} = D_s \frac{\partial^2 T}{\partial z^2} \quad \text{for } z \leq 0; \quad \frac{\partial T}{\partial t} = D_i \frac{\partial^2 T}{\partial z^2} \quad \text{for } 0 \leq z \leq h(t) \quad (4.1)$$

where $D_{s,i}$ are the heat diffusion coefficients in the substrate and the ice respectively. These equations have to be solved with regards to the following boundary conditions at the two interfaces, firstly $z = 0$:

$$T(0^-, t) = T(0^+, t); \quad \lambda_s \frac{\partial T}{\partial z}(0^-, t) = \lambda_i \frac{\partial T}{\partial z}(0^+, t). \quad (4.2)$$

These conditions impose both the continuity of the temperature and the heat flux at the solide/ice interface, $\lambda_{s,i}$ being the thermal conductivity of the substrate material and the ice respectively. For $z = h(t)$, we have:

$$T(h(t)^-, t) = T_m; \quad \lambda_i \frac{\partial T}{\partial z}(h(t)^-, t) = \rho_i L \frac{dh}{dt}. \quad (4.3)$$

which corresponds to the continuity of the temperature and the Stefan condition at the solidification front. The Stefan condition imposes here that the cold heat flux coming from the ice is totally transferred into the water-ice phase change. Finally, we impose also a boundary condition for the substrate temperature far from the interface : $\lim_{z \rightarrow -\infty} T(z, t) = T_s$ and we complement this set of equations by the initial conditions taken at $t = 0$:

$$T(z, 0) = T_s \text{ for } z \leq 0 \text{ and } h(0) = 0, \quad (4.4)$$

indicating that at $t = 0$ the solid and the liquid are suddenly in contact. To the best of our knowledge, we are not aware of such system of equations modeling ice growth by a sudden contact between a liquid and a solid substrate. In fact, multilayer heat transfers with solidification/fusion have been considered numerically in the case of laser heating of nanoscale metal films, leading to similar set of equations, but with different boundary/initial conditions (Font *et al.* 2017).

Similarity analysis shows that this diffusive problem keeps its self-similar behavior, with the self-similar variable $\eta = \frac{z}{\sqrt{t}}$, even in the presence of the moving solidification front. In this case, the solidification front obeys following diffusive law :

$$h(t) = \sqrt{D_{\text{eff}} t} \quad \text{with} \quad D_{\text{eff}} = 4\beta^2 D_i \quad (4.5)$$

where we introduce the Stefan number:

$$\text{St} = \frac{C_{pi} \Delta T}{L}, \quad (4.6)$$

with C_{pi} the heat capacity of ice and L the latent heat of solidification. St compares the heat transfer from the water/ice interface to the substrate with the latent heat released at solidification. This notation is reminiscent of the Stefan problem (Worster 2000). D_{eff} is the effective diffusion coefficient, it really is the quantity of interest of our problem as it controls the ice growth. It corresponds to the diffusive coefficient of ice weighted by the Stefan number and β a function of the Stefan number and of the other thermal parameters. β goes to 1 if the properties of the substrate approach those of ice, so that the solution of Stefan problem, with infinite ice is recovered.

Introducing the self-similar variable in the set of Equations (4.1)–(4.4), we obtain the following solution for the problem :

$$T(z, t) = T_0 + (T_0 - T_s) \cdot \text{Erf}\left(\frac{z}{2\sqrt{D_s t}}\right) \text{ for } z \leq 0 \text{ and} \quad (4.7)$$

$$T(z, t) = T_0 + \frac{e_s}{e_i} (T_0 - T_s) \cdot \text{Erf}\left(\frac{z}{2\sqrt{D_i t}}\right) \text{ for } 0 \leq z \leq h(t) \quad (4.8)$$

where T_0 , the temperature at the ice/substrate interface (a constant in time) and A are integration constant, and the error function Erf is defined by:

$$\text{Erf}(x) = \frac{2}{\sqrt{\pi}} \int_0^x e^{-\xi^2} d\xi \quad (4.9)$$

Writing the Stefan flux condition for $z = h(t)$ (4.3) we obtain the transcendental equation for β :

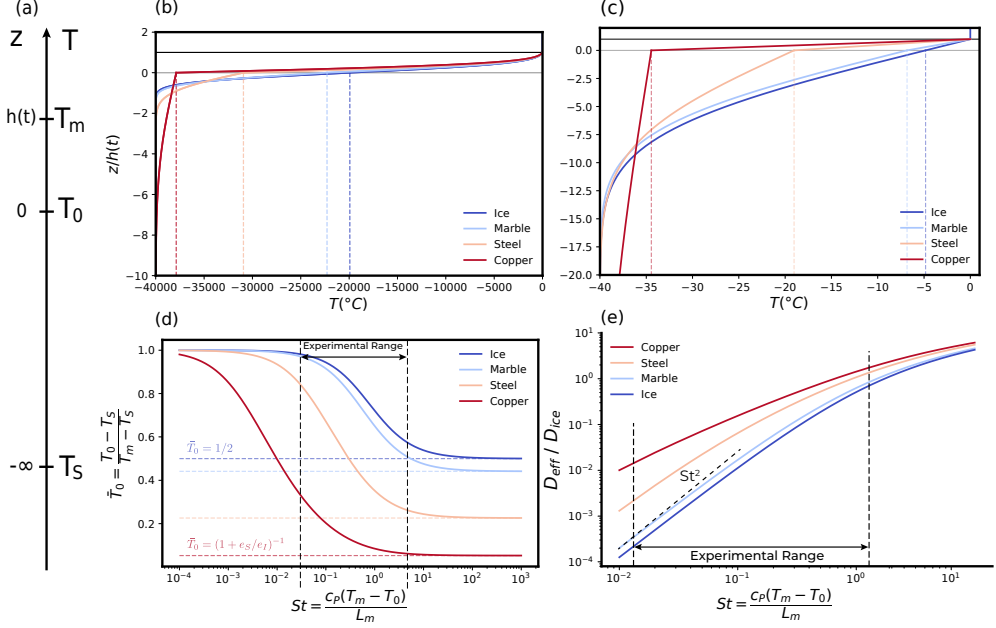


FIGURE 3. Results of the model for the different substrates (copper: red, steel: orange, marble: light blue) and ice (dark blue) that is for comparison with the Stefan problem with infinite ice and infinite liquid water. (a) Schematic of the problem with its boundary conditions in $z = h(t)$ and $z = -\infty$. (b) & (c): Temperature profiles obtained from eq. 4.8 and 4.7. The altitude is normalized by the thickness of the growing ice layer, showing that the thermal boundary layer in the substrate is several times thicker than the ice layer. (b) For $St = 250$. This case is non physical for water, as the substrate would need to be -40.000°C . However it shows the theoretical asymptotic regime for $St \gg 1$. We can see the shape of the erf function profile within both phases: the ice and the substrate. The temperature gradient is discontinuous at the contact between the ice and the substrate, because of the discontinuity in the thermal conductivity. This causes the break in the slope at $z=0$. (c) Same for $St = 0.25$, which falls within the temperature range of our experiments. The temperature profile tends to be linear in the ice. (d) Dimensionless contact temperature, obtained from eq. 4.11. Regardless of the substrate, it goes to 1 for $St \ll 1$, meaning that if thermal transfer is dominated by latent heat, the contact temperature is the melting point. For $St \gg 1$, \bar{T}_0 goes the asymptotical value $(1 + e_s/e_i)^{-1}$ which is known as the contact temperature of two infinite bodies initially at different temperatures and depends on their thermal effusivities. (e) Effective diffusion coefficient D_{eff} of the solidification front normalised by the thermal diffusion coefficient of the ice D_{ice} , as a function of the Stefan number. The differences between substrates are more important at low Stefan number, and there is an asymptotical regime as St^2 (dashed line).

$$St = \sqrt{\pi} \beta e^{\beta^2} \left(\frac{e_I}{e_s} + \text{Erf}(\beta) \right) \quad (4.10)$$

where the $e_{s,i} = \sqrt{\lambda_{s,i} \rho_{s,i} C_{ps,i}}$ are the so called effusivities of the materials.

Finally, by writing the temperature at $z=h(t)$, we express the normalized temperature of the ice/substrate interface as a function of β :

$$\bar{T}_0 = \frac{T_0 - T_s}{T_m - T_s} = \frac{1}{1 + \frac{e_s}{e_i} \text{Erf}(\beta)} \quad (4.11)$$

The normalized temperature profiles are plotted on figure 3(b) and (c), respectively

for $St = 250 \gg 1$ and $St = 0.25 \sim 1$, and for our three different materials used in our experiment. The case where ice, with a given temperature, is used as a substrate, has been added. Note that in our experiment, these Stefan numbers correspond respectively to a substrat temperature T_s equal to -40000°C , far below the absolute zero, and to -40°C the middle of our experimental range. The profiles evolves from the substrat temperature T_s up to the solidification temperature $T_m = 0^\circ\text{C}$. In addition, figure 3(d) and (e) present respectively the normalized temperature \bar{T}_0 (Eq. 4.11) and the normalized effective diffusion coefficient D_{eff}/D_i (Eq. 4.5), plotted as a function of the Stefan number, for the three different materials used in our experiment, and for ice as a substrat. Note that increasing the Stefan numbers correspond to decrease the substrat temperature. Our experimental temperature range is shown on the graphs, between $St = 10^{-2}$ which corresponds roughly to a 1°C temperature difference between the substrat and the front, and $St = 1$ is for temperature difference close to a hundred.

Let us first consider the theoretical case of large Stefan numbers : $St \gg 1$. In this asymptotic regime : $C_p \Delta T \gg L$, meaning that the heat (L), released by the solidification at the water/ice interface ($h(t)$) is negligible compared to the heat energy needed to warm the ice up ($C_p \Delta T$). This explains the symmetrical Erf shape of the temperature profil in the ice. For the other materials, two Erf functions also join at the ice/substrat interface, but the symmetry is broken by the interface temperature which is not simply the average of T_m and T_s but is given by the interface temperature of two infinite medium in contact (de Ruiter *et al.* 2018) :

$$T_{0, St \gg 1} = T_s + (T_m - T_s) \frac{1}{1 + \frac{e_s}{e_i}}$$

which corresponds to Eq. 4.11 evaluated for large Stefan number. These interface temperatures are the asymptotic temperatures for large Stefan numbers on figure 3(d). In this case, the effective diffusion coefficient (figure 3(e)) of all of our substrats are close to the one without substrat (ice curve) as the substrat does not influence much the solidification front propagation.

When the Stefan number decreases and approaches 1, the heat supplied by the solidification becomes comparable to the one consumed by the ice. As a consequence, the temperature profile in the ice becomes almost linear (figure 3(c)) and join an Erf function which goes deeper in the substrat compared to the large Stefan regime. The solidification is now efficient enough to warm the substrate up. For that reason, the normalized interface temperature T_0 also influenced by the solidification increases (figure 3(d)) to be now between T_m and $T_{0, St \gg 1}$. The effective diffusion coefficient is obviously smaller than in the large Stefan regime because the substrate temperature is smaller. What is more interesting is that D_{eff} for metal substrate get away from the one of the ice, because the solidification front propagation becomes more influenced by the substrate thermic parameters as the Stefan number decreases : the higher the substrate thermal conductivity, the faster the solidification front propagation.

Finally for $St \ll 1$, the relatively large heat flux supplied by the solidification front, crosses the ice without being much consumed. The larger part of the latent heat is used to warm the substate up and T_0 becomes very close to T_m . In the figure 3(e), the dotted line shows the asymptotic behavior at low Stefan number : $D_{\text{eff}}/D_i \propto St^2$.

5. The ice pancake

At this point, we know the time during which the ice pancake is building (τ_{SCL}) and we have a model for the ice growth (D_{eff}) ; we now need the experimental thickness

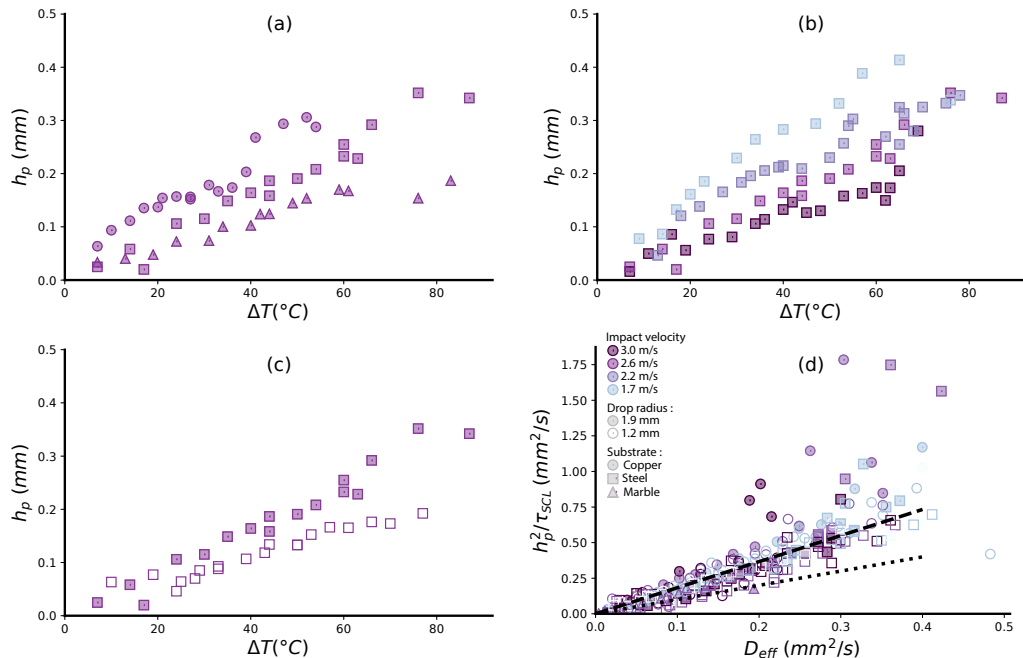


FIGURE 4. (a) Evolution of the underlying ice plate thickness h_p as a function of the temperature ΔT , for different substrates, with the same impact velocity (2.6 m/s) and drop radius (1.9 mm). h_p increases as the substrate temperature decreases (that is when ΔT increases), which is logical: the colder the substrate, the more ice will freeze during the time τ_{SCL} . At a given temperature the more conductive substrate (copper, in circles) freezes more ice than the less conductive substrate (marble, in triangles). (b) Evolution of h_p along ΔT for different impact velocities, on the same substrate (steel) and with the same drop radius (1.9mm). For a given temperature, a thicker layer of ice is frozen for the lowest impact velocities (in light blue) than for the highest (in deep purple). It is due to the change in the time of residence, shown in Fig. 2. For lower velocities the water freezes during a longer time and thus freezes more. (c) Evolution of h_p with ΔT for different drop radius, on the same substrate (steel) and at the same velocity (2.6 m/s). It shows that the smaller the drop the less it freezes. (d) Rescaling of the measurements against the model: the measured diffusivity and the solidification front, h_p^2/τ_{SCL} is plotted against the effective diffusion coefficient obtained through the previously described model (Eq. 4.5 and 4.10). It shows a good collapse for all experiments, regardless of the substrate (symbols), impact velocity (colour) or drop size (full or empty symbols). The thick dashed line is a linear fit of the data points, showing a slope of 1.8. The thin dashed line has a slope 1 as predicted by the model.

of the pancake (h_p) to put our model to a test. Figures 4(a)-(c) show the experimental measurement of h_p deduced from the height profiles of the frozen drops (see Fig. 1(i)), as a function of ΔT , respectively for four different drop velocities (a), three different substrates (b) and two different drop sizes (c). These control parameters, and their corresponding markers, are the same as those used in figure 2.

These figures show that the underlying ice layer becomes thicker in the following cases. First, when the substrate gets colder (Fig. 4(a)-(c)) : more liquid can be frozen during the solidification time that appeared to be mostly constant with ΔT (fig 2(b)-(c)). Then, as the substrate heat conductivity increases (fig. 4(a)): as heat energy is sucked with higher efficiency, the freezing front can propagate faster during a solidification time that does not vary much (fig 2(d)). Lastly, as the drop velocity is slower fig. 4(b) and as the drop

size is smaller (fig. 4(c)): the slower or the smaller the impacting drop, the longer the spread drop stays freezing before retracting (fig 2(c)).

We can now compare these experimental results to our model. Figure 4 (d) presents the variation of h_p^2/τ_{res} , which represents the experimental diffusivity of the solidification front within the time of residence τ_{SCL} , as a function of the effective diffusion coefficient D_{eff} determined by our model, for all the substrate materials, substrate temperatures, drop sizes and impact velocities investigated experimentally. We observe a nice collapse of all the data into a straight line. This indicates clearly that our simplified 1D model account well for this problem and that the ice pancake formation is controlled by the coupling of the thermal diffusion with the depinning time of the remaining liquid film.

The collapsed data lie along a line with a slope of 1.8, above the thick dashed line of slope 1 on the figure. We can therefore conclude that the ice pancake thickness is well described by the expression :

$$h_p^2 \simeq 1.8 D_{\text{eff}} \tau_{\text{res}}$$

The slightly greater than one pre-factor indicates that the actual growth of the ice layer is faster than what our model predicts, in other words the thermal transfer in our experiment is more efficient than in the 1D model. This might be due to the three-dimensional shape of the freezing drop which is not taken into account in the one-dimensional model. In the 3D case, the drop will have a finite radius and the substrate will be infinitely wide, so that radial diffusion in the substrate can add up to vertical diffusion and speed up the whole process of freezing.

We observe that some experiments are not collapsing on the line with the others. They appear particularly for an effective diffusive coefficient greater than $2.10^{-7} \text{ m}^2/\text{s}$. This limit of our model probably comes from the hypothesis of semi-infinite water in the freezing model. Indeed if we estimate the thickness of the freezing water film with the drop volume V_0 and the spreading radius R_{max} , we find $h_f \sim V_0/\pi R_{\text{max}}^2$. With a drop of volume $V_0 = 30\mu\text{L}$ spreading to a radius of $R_{\text{max}} = 7\text{mm}$, we obtain $h_f \sim 200\mu\text{m}$ which corresponds to highest values of h_p . Thus if the whole film freezes at once, the hypothesis of semi-infinite water does not hold anymore.

6. Conclusion

Though this behaviour remains mysterious, we can propose several ideas about the origin of the time of residence. As it appears on Figure 2a, the residence regime is the only difference between the cases with and without solidification. Particularly, the retraction velocity is the same regardless of the temperature. This supports the idea that the retraction is controlled by viscosity and capillarity. Therefore during the residence regime, we would expect the contact angle θ to decrease from an advancing angle θ_a to a receding angle θ_r in order to enable the retraction. The time of residence would then be the characteristic time of the contact angle dynamic. On the variation of the time of residence with the height of fall of the drop, one should recall that the higher the drop falls, the further it spreads. Considering the spread drop to be a cylindrical film and keeping the initial drop volume constant, it means its thickness becomes thinner for higher velocities, and so a more important fraction of it is frozen at the impact. In other words, the higher the impact velocity, the lesser liquid will remain to retract. So the freezing upon impact acts as if the drop was spread with a more important aspect ratio, whence the contact angle will be smaller and thus closer to its receding value. As a result of this reasoning, the contact angle at the beginning of the residence regime should be smaller for the higher velocities, which is coherent with the experimental results of figure

2. Unfortunately one cannot easily define contact angles in the presence of solidification, both theoretically for there is no thermodynamic equilibrium, and experimentally since we could not measure the dynamic of the contact angle. For that reason, we will not conclude on the origin of the residence regime and we will focus on the formation of the ice layer during that time.

We assume that this variation of SCL time with the substrate is rather due to the different wetting angle, which might changes the maximum spreading diameter, than the difference in heat transfert.

7. Acknowledgements

REFERENCES

- BARTOLO, DENIS, JOSSERAND, CHRISTOPHE & BONN, DANIEL 2005 Retraction dynamics of aqueous drops upon impact on non-wetting surfaces. *J. Fluid Mech.* **545**, 329–338.
- BAUMERT, A., BANSMER, S., TRONTIN, P. & VILLEDIEU, P. 2018 Experimental and numerical investigations on aircraft icing at mixed phase conditions. *Int. J. Heat Mass Transf.* **123**, 957–978.
- DERBY, B. 2010 Inkjet printing of functional and structural materials: fluid property requirements, feature stability and resolution. *Annu. Rev. Mater. Res.* **40**, 395–414.
- FONT, F., AFKHAM, S. & KONDIC, L. 2017 Substrate melting during laser heating of nanoscale metal films. *Int. J. Heat Mass Transf.* **113**, 237–245.
- GAO, FUQUAN & SONIN, AIN A 1994 Precise deposition of molten microdrops: the physics of digital microfabrication. In *Proc. R. Soc. Lond. A*, , vol. 444, pp. 533–554. The Royal Society.
- GHABACHE, ELISABETH, JOSSERAND, CHRISTOPHE & SÉON, THOMAS 2016 Frozen impacted drop: From fragmentation to hierarchical crack patterns. *Physical Review Letters* **117** (7), 074501.
- GUPTA, S.C. 2003 *The Classical Stefan Problem - Basic Concepts, Modelling and Analysis*. Elsevier Science B.V, Amsterdam.
- HAUK, T., BONACCURSO, E., ROISMAN, I.V. & TROPEA, C. 2015 Ice crystal impact onto a dry solid wall. particle fragmentation. *Proc. R. Soc. A* **471**, 20150399.
- JOSSEAND, C & THORODDSEN, ST 2016 Drop impact on a solid surface. *Annual Review of Fluid Mechanics* **48**, 365–391.
- LAAN, NICK, DE BRUIN, KARLA G, BARTOLO, DENIS, JOSSEAND, CHRISTOPHE & BONN, DANIEL 2014 Maximum diameter of impacting liquid droplets. *Physical Review Applied* **2** (4), 044018.
- MARIN, ALVARO G, ENRIQUEZ, OSCAR R, BRUNET, PHILIPPE, COLINET, PIERRE & SNOELJER, JACCO H 2014 Universality of tip singularity formation in freezing water drops. *Physical review letters* **113** (5), 054301.
- RIVETTI, MARCO, SALEZ, THOMAS, BENZAQUEN, MICHAEL, RAPHAËL, ELIE & BÄUMCHEN, OLIVER 2015 Universal contact-line dynamics at the nanoscale. *Soft Matter* **11** (48), 9247–9253.
- DE RUITER, JOLET, SOTO, DAN & VARANASI, KRIPA K 2018 Self-peeling of impacting droplets. *Nature Physics* **14** (1), 35.
- SCHIAFFINO, STEFANO & SONIN, AIN A. 1997 Motion and arrest of a molten contact line on a cold surface: An experimental study. *Physics of Fluids* **9** (8), 2217–2226.
- SCHREMB, M., ROISMAN, I.V. & TROPEA, C. 2018 Normal impact of supercooled water drops onto a smooth ice surface: experiments and modelling. *J. Fluid Mech.* **835**, 1087–1107.
- SNOELJER, JACCO H & BRUNET, PHILIPPE 2012 Pointy ice-drops: How water freezes into a singular shape. *American Journal of Physics* **80** (9), 764–771.
- STEFAN, J. 1891 Über die theorie der eisbildung, insbesondere über die eisbildung im polarmeere. *Ann. Physik Chemie* **42**, 269–286.

- VIDAURRE, G. & HALLETT, J. 2009 Particle impact and breakup in aircraft measurement. *J. Atmos. Ocean. Technol.* **26**, 972–983.
- WILDEMAN, S., STERL, S., SUN, C. & LOHSE, D. 2017 Fast dynamics of water droplets freezing from the outside in. *Phys. Rev. Lett.* **118**, 084101.
- WORSTER, M.G. 2000 *Perspectives in Fluid Dynamics — a Collective Introduction to Current Research*, chap. Solidification of Fluids. Cambridge Univ. Press.